Chemical Science

ROYAL SOCIETY OF CHEMISTRY

EDGE ARTICLE

View Article Online
View Journal | View Issue

Cite this: *Chem. Sci.*, 2020, **11**, 7871

All publication charges for this article have been paid for by the Royal Society of Chemistry

Interrogating surface *versus* intracellular transmembrane receptor populations using cell-impermeable SNAP-tag substrates†

Pascal Poc, ‡[a] Vanessa A. Gutzeit,‡[b] Julia Ast, ‡[cd] Joon Lee, ‡[e] Ben J. Jones, [f] Elisa D'Este, [g] Bettina Mathes,[a] Martin Lehmann,[h] David J. Hodson, *[cd] Joshua Levitz*[ei] and Johannes Broichhagen §*[aj]

Employing self-labelling protein tags for the attachment of fluorescent dyes has become a routine and powerful technique in optical microscopy to visualize and track fused proteins. However, membrane permeability of the dyes and the associated background signals can interfere with the analysis of extracellular labelling sites. Here we describe a novel approach to improve extracellular labelling by functionalizing the SNAP-tag substrate benzyl guanine ("BG") with a charged sulfonate ("SBG"). This chemical manipulation can be applied to any SNAP-tag substrate, improves solubility, reduces non-specific staining and renders the bioconjugation handle impermeable while leaving its cargo untouched. We report SBG-conjugated fluorophores across the visible spectrum, which cleanly label SNAP-fused proteins in the plasma membrane of living cells. We demonstrate the utility of SBG-conjugated fluorophores to interrogate class A, B and C G protein-coupled receptors (GPCRs) using a range of imaging approaches including nanoscopic superresolution imaging, analysis of GPCR trafficking from intra- and extracellular pools, *in vivo* labelling in mouse brain and analysis of receptor stoichiometry using single molecule pull down.

Received 15th May 2020
Accepted 2nd July 2020

DOI: 10.1039/d0sc02794d

rsc.li/chemical-science

Introduction

Membrane receptors, including ligand-gated ion-channels, G protein-coupled receptors (GPCRs), receptor-linked enzymes and, to an extent, transporters, sense extracellular stimuli and convert them into intracellular signals that control cellular function in myriad ways.[1] As such, these proteins are a major focus of drug discovery programs, with GPCRs serving as the largest class of targets.[2] Through an array of approaches it has become clear that receptor signalling is not restricted to the cell surface but is fine-tuned by a dynamic interplay of receptors both on the surface and in intracellular compartments.[3–6] Developing techniques for dissecting the relative properties of these distinct pools is an emerging challenge for receptor biology.

Fluorescence microscopy is a powerful technique for direct observation and analysis of molecular processes within a living cell that has been applied extensively to the study of membrane receptors. The continuing development of bright and stable synthetic dyes[7–10] along with the engineering of self-labelling suicide enzymes, such as SNAP, CLIP and Halo-tags,[11] has spurred the application of targeted, high-resolution imaging in a number of biological contexts.[12–21] Organic dyes that are covalently linked to proteins offer superior brightness, photostability and flexibility compared to fluorescent proteins.[10,22] Many organic dyes are cell permeable and therefore suitable for intracellular labelling. However, this permeability is undesirable when cell surface targeting is required since confounding background signals can arise from labelled, un-trafficked proteins or accumulation of the unlabelled dye in membranes and intracellular compartments. Similarly, fluorescent protein-tagged membrane proteins tend to give high background

[a]*Max Planck Institute for Medical Research, Department of Chemical Biology, Jahnstr. 29, 69120 Heidelberg, Germany*
[b]*Neuroscience Graduate Program, Weill Cornell Medicine, New York, NY 10065, USA*
[c]*Institute of Metabolism and Systems Research (IMSR), Centre of Membrane Proteins and Receptors (COMPARE), University of Birmingham, Birmingham, UK*
[d]*Centre for Endocrinology, Diabetes and Metabolism, Birmingham Health Partners, Birmingham, UK*
[e]*Department of Biochemistry, Weill Cornell Medicine, New York, NY 10065, USA*
[f]*Section of Investigative Medicine, Imperial College London, London W12 0NN, UK*
[g]*Optical Microscopy Facility, Max Planck Institute for Medical Research, Heidelberg, Germany*
[h]*Leibniz-Forschungsinstitut für Molekulare Pharmakologie (FMP), Department of Pharmacology and Cell Biology, Robert-Rössle-Str. 10, 13125 Berlin, Germany*
[i]*Tri-Institutional PhD Program in Chemical Biology, New York, NY 10065, USA*
[j]*Leibniz-Forschungsinstitut für Molekulare Pharmakologie (FMP), Department of Chemical Biology, Robert-Rössle-Str. 10, 13125 Berlin, Germany. E-mail: broichhagen@fmp-berlin.de*

† Electronic supplementary information (ESI) available. See DOI: 10.1039/d0sc02794d

‡ These authors contributed equally.

§ Lead contact.

signals when fused to membrane proteins, since they are expressed, translated and trafficked within the cell. While membrane impermeable fluorophores exist (*e.g.* Alexa, Atto or Abberior dyes), many of these fluorophores have been shown to accumulate at the membrane.[23] In addition, the recently developed bright and stable Janelia Fluors[24] and MaP dyes[8] are engineered to be membrane permeable making them difficult to apply to studies of surface proteins. So far, the membrane permeability of a probe has been considered a feature of the fluorophore, with the consequence that imaging only the extracellular protein pool requires changing to a spectrally and photophysically distinct dye, as shown recently.[25] While generally useful for qualitative analysis, such an alteration makes quantitative comparisons difficult. Thus, a strategy for rendering dyes impermeable without altering their intrinsic photophysical or spectral properties is needed.

Herein, we describe a subtle, yet powerful modification of O^6-benzylguanine (BG), the substrate for the SNAP-tag, by installing a sulfonate on the leaving group's C8 position (termed SBG), rendering them impermeable towards the lipid bilayer while conserving reactivity with SNAP. Our general approach allows clean surface labelling of GPCRs in living cells with improved membrane localization and resolution by STED nanoscopy, as well as enhanced signal-to-noise ratio and spread *in vivo*. Moreover, SBG-linked fluorophores open up the possibility to pulse-chase receptors in different compartments, as well as to perform single molecule pulldown (SiMPull) studies of surface *versus* intracellular receptor populations. We anticipate that with this facile strategy the majority of linked substrates can be rendered impermeable for studies of membrane protein dynamics at the cell surface.

Results

As a proof-of-principle, we first set out to design and synthesize membrane impermeable versions of SNAP-Cell® TMR-Star and SNAP-Cell® 647-SiR, two popular commercially-available fluorophores for SNAP-tag labelling (Fig. 1a). Based on previous studies, which report that alterations at guanine position C8 are tolerated for enzymatic SNAP labelling,[26] we hypothesized that substituents on the BG would alter the permeability of the entire compound without interfering with labelling. Conveniently, this moiety would also be liberated upon SNAP labelling, thus removing any potential alterations to the photophysical properties of the protein-bound fluorophore itself. As such, three moieties were examined as their TMR- and SiR-bearing reagent, namely the parent BG (with H at C8: "BG-TMR" and "BG-SiR"), a previously described[26] carboxylate CBG (with a linked COOH at C8: "CBG-SiR") and, finally a sulfonate (with a linked SO_3H at C8: "SBG-TMR" and "SBG-SiR") (Fig. 1b, c and Schemes S1, S2†). Bearing in mind that sulfonates display a $pK_a < 0$, SBG will be permanently negatively charged in physiological buffers, thereby unable to cross the lipid bilayer membrane and, presumably, repelled further by the negatively charged surface. Accordingly, CBG-SiR, SBG-TMR and SBG-SiR were prepared and obtained by straightforward amide coupling of CBG- and SBG-amines to NHS-activated fluorophores (see ESI†).

For initial assessment of labelling properties, we chose TMR since covalent binding of a non-fluorogenic dye can easily be observed using fluorescence polarization. As expected, BG-TMR and SBG-TMR showed complete SNAP labelling *in vitro* as assessed by full protein mass spectrometry[27] (Fig. S1–S3†) with labelling kinetics ~3-times slower for SBG-TMR ($t_{1/2}$ = 51.3 seconds) *versus* BG-TMR ($t_{1/2}$ = 17.8 seconds) yet complete within minutes (Fig. S4a†). An advantage of using a charged residue is increased solubility, and as such, SBG-TMR can be readily dissolved in pure PBS at a concentration ≥1.5 mM, while BG-TMR need to be dissolved in DMSO (≥1 mM) before dilution in PBS for usage. More importantly, BG-TMR (~80 μM in PBS, 1% DMSO) was not stable in solution at room temperature, precipitating within minutes to leave a steady-state concentration of ~17 μM in the supernatant (Fig. S4b†). Notably, SBG-TMR remained in solution at ~70 μM without the addition of DMSO over three days (Fig. S4b†).

We next tested the ability of modified BGs to label intracellular SNAP by expressing either a cytosolic- or nuclear-targeted SNAP-tag before applying BG, CBG or SBG-conjugated fluorophores. While labelling with 500 nM BG-SiR for 45 minutes at 37 °C produced clear fluorescence for both cytosolic and nuclear SNAP-tags, labelling with 500 nM CBG-SiR or SBG-SiR did not produce any substantial signal with either construct in transiently transfected HEK 293 cells (Fig. 1d and e). Notably, background fluorescence in untransfected cells was highest for BG-SiR, lower for CBG-SiR and undetectable for SBG-SiR (Fig. 1d and e). As such, we decided to continue our characterization with SBG-SiR because it showed a robust decrease in membrane permeability compared to CBG-SiR. We next labeled cells expressing a SNAP-tagged GPCR, metabotropic glutamate receptor 2 ("SNAP-mGluR2"), with either BG-SiR or SBG-SiR. Both compounds produced clear fluorescence over a similar range of labelling concentrations (Fig. 1f and g), but signals from SBG-SiR were more confined to the plasma membrane (Fig. 1f, right) and showed less background labelling in untransfected cells (Fig. 1g and h). Together, these data validate the idea that addition of an anionic sulfonate group to BG can render an attached fluorophore membrane-impermeable for targeting of surface proteins with reduced non-specific labelling.

Due to their distinct spectral and photophysical properties, different fluorophores are required for multimodal applications. Based on the desire to prevent membrane permeability of different fluorophores at will, we asked if this approach was generalizable to a family of fluorophores spanning visible to far-red wavelengths. To do this, we synthesized and tested SBG-conjugated Oregon Green (OG), TMR, Janelia Fluor 549 (JF_{549}) and Janelia Fluor 646 (JF_{646}) (Fig. 2a–d), the latter showing superior brightness and photostability over their tetramethyl and silicon rhodamine counterparts.[24] In all cases, SBG-conjugated fluorophores clearly label surface receptors, with minimal labelling of intracellular SNAP-tags (Fig. 2a–d). Furthermore, fluorescence lifetimes of BG- and SBG-JF_{549} were similar following labelling of cells expressing SNAP-tag

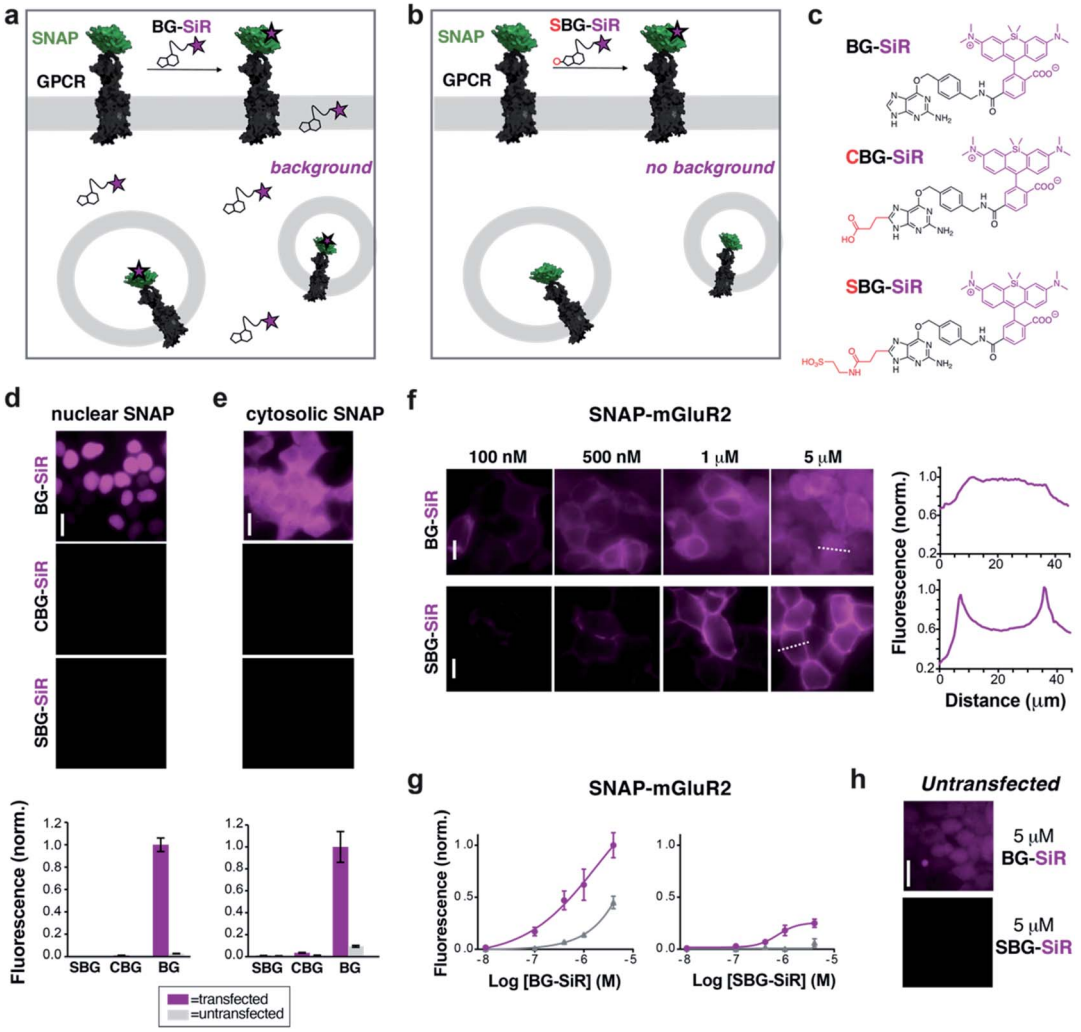

Fig. 1 CBG and SBG-conjugated SiR are membrane-impermeable and enable specific targeting of surface proteins. (a) Application of permeable BG-SiR to N-terminally SNAP-fused GPCRs leads to extracellular labelling of surface receptors and background signals due to labelling of intracellular pools and non-specific dye accumulation. (b) Application of impermeable SBG-SiR should lead solely to labelling of extracellular tags with reduced background. (c) Chemical structures of BG-SiR, CBG-SiR and SBG-SiR. (d and e) BG-SiR, but not CBG-SiR and SBG-SiR, labels nucleus-targeted (d) or cytosol-targeted (e) SNAP-tags. Labelling concentration was 500 nM for all compounds. (f and g) Concentration-dependent labelling of SNAP-mGluR2 leads to intracellular background signals using BG-SiR, which is absent using SBG-SiR. Line scans, right, demonstrate that labelling restricted to the surface only with SBG-SiR. (h) Untransfected cells show background signals from BG-SiR but not from SBG-SiR. Scale bars are 20 μm.

(Fig. S5†). Thus, modification of the BG with sulfonate does not markedly influence post-labelling photophysical dye properties.

To test if membrane-localized SNAP-tag labels offer advantages for cell biology, we turned to nanoscopic STED imaging. A dye with outstanding far-red performance in STED microscopy with respect to photostability and brightness is JF_{646}.[28] Accordingly, we used JF_{646} SNAP-tag probes to target SNAP-mGluR2 in transiently transfected HEK 293 cells. Similar to what was observed by widefield microscopy (Fig. 2d), we observed mainly intracellular staining in fixed cells with BG-JF_{646} (Fig. 2e). This intracellular fluorescence is likely due to a mixture of immature proteins that have not yet trafficked to the cell surface and surface receptors that have been internalized. By instead using SBG-JF_{646}, we obtained images where the dye remained solely at the cell surface, and furthermore, were able to resolve membranes with a lateral resolution of 91 ± 23 nm using STED nanoscopy ($n = 42$; *cf.* $FWHM_{confocal} = 295 \pm 85$ nm, $n = 35$) (Fig. 2f).

We next asked if SBG-conjugated fluorophores could allow for superior labelling of GPCRs *in vivo*. We recently established SNAP-tag labelling *in vivo* in the frontal cortex of living mice using local injection of BG-conjugated fluorophores.[29] Presumably, the high solubility and reduced cell permeability of SBG-conjugated fluorophores should lead to improved tissue staining. Based on our prior study, we virally-delivered SNAP-mGluR2 into the medial prefrontal cortex (mPFC) of adult mice before injecting BG-JF_{549} or SBG-JF_{549} 8 weeks later at the same coordinates (Fig. 3a). Clear labelling was observed with both compounds (Fig. 3b–g), but we observed a larger spread of SBG-JF_{549} fluorescence in transduced brains (Fig. 3d and S6†)

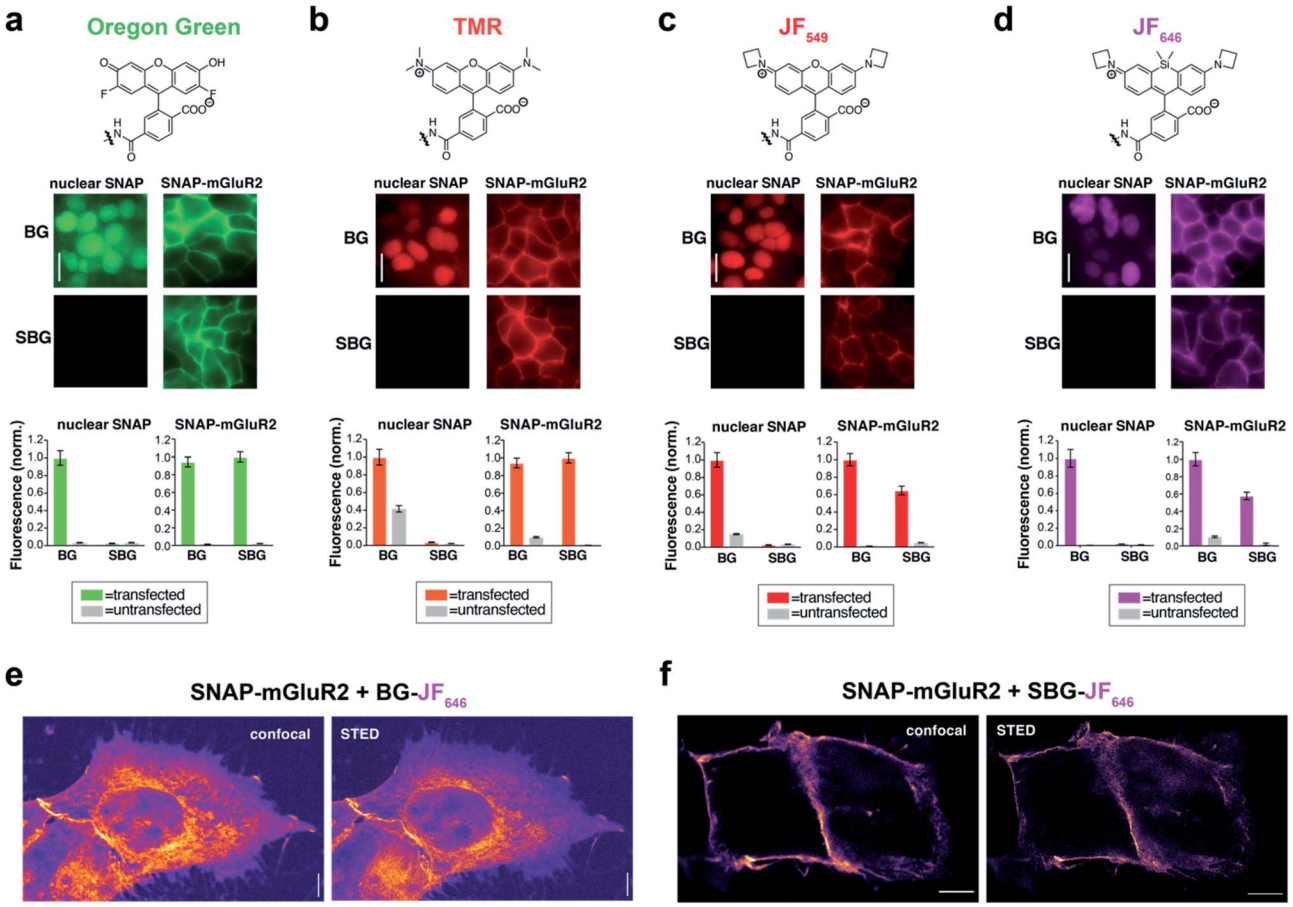

Fig. 2 SBG-conjugated fluorophores across the visible spectrum enable surface-specific SNAP labelling and nanoscopic imaging of surface receptors. (a–d) SBG conjugation enables surface targeting of Oregon Green (a), TMR (b), JF_{549} (c), and JF_{646} (d). All fluorophores label nuclear SNAP-tags when conjugated BG but not SBG, for which they show cleaner surface targeting of SNAP-mGluR2. (e and f) Confocal and super-resolution STED nanoscopy of mGluR2 using BG-JF_{646} (e) and SBG-JF_{646} (f) shows clear isolation of the membrane population only using the impermeable SBG probe. Labelling concentration was 500 nM for all compounds. Data is represented as mean ± SEM. Scale bars are 20 μm.

and untransduced brains showed a 2-fold higher background for BG-JF_{549} than its SBG counterpart (Fig. 3g).

Having established efficient surface-targeted labelling with SBG-conjugated fluorophores, we next asked if we could use BG- and SBG-conjugated fluorophores to separate the intra- and extracellular pools of a membrane receptor, a challenging feat with conventional approaches. We employed glucagon-like peptide-1 receptor N-terminally fused to SNAP ("SNAP-GLP1R"), and used two spectrally separated dyes to pulse-chase label different receptor pools (Fig. 4a). GLP1R is involved in glucose homeostasis[30] and is known to undergo rapid endocytosis and trafficking upon activation with the agonist exendin 4(1–39) (Ex4). Tracking of surface-exposed receptors has previously been achieved by using BG-Alexa or BG-Atto dyes in plate-reader experiments or fixed cells[31,32] or by the use of specific antibodies.[30,32] However, none of these studies attempted to simultaneously resolve the behaviour of surface and intracellular receptor populations in the same living cells.

We therefore set out to achieve this high bar, by combining SBG- and BG-conjugated fluorophores. Cells were initially incubated with SBG-TMR (500 nM) to label SNAP-GLP1R at the cell surface, followed by application of BG-SiR (500 nM) (Fig. 4a). After washing, SNAP-GLP1R was clearly labelled at the surface with TMR and intracellularly with SiR (Fig. 4b). While a population of surface receptor was also labelled by BG-SiR, this likely reflects newly trafficked (*i.e.* during the 10 minute wash step) or residual GLP1R (*i.e.* unlabelled by SBG-TMR). Pertinently, no bleedthrough was apparent in controls that used a single dye (Fig. S7†). SBG-TMR labelling was relatively homogenous and uniform in CHO_SNAP-GLP1R cells under non-stimulated conditions (Fig. 4c), as expected with stable transfection. Surface SNAP-GLP1R was activated by exendin 4(1–39) (Ex4; 25 nM), before tracking of TMR and SiR-labelled receptor pools in live cells at high resolution (Fig. 4b). After 15 minutes of agonist treatment, cells were washed and the antagonist exendin 4(9–39) (Ex9; 500 nM) was applied to allow the internalized and cytosolic receptors pools to be sorted and re-trafficked to the surface (Fig. 4b). As expected, TMR-labelled GLP1R readily internalized following ligand binding, before trafficking and degradation upon washout and application of antagonist, as evaluated by mean fluorescence intensity at the membrane and in the cytosol (Fig. 4d and e). Interestingly, we

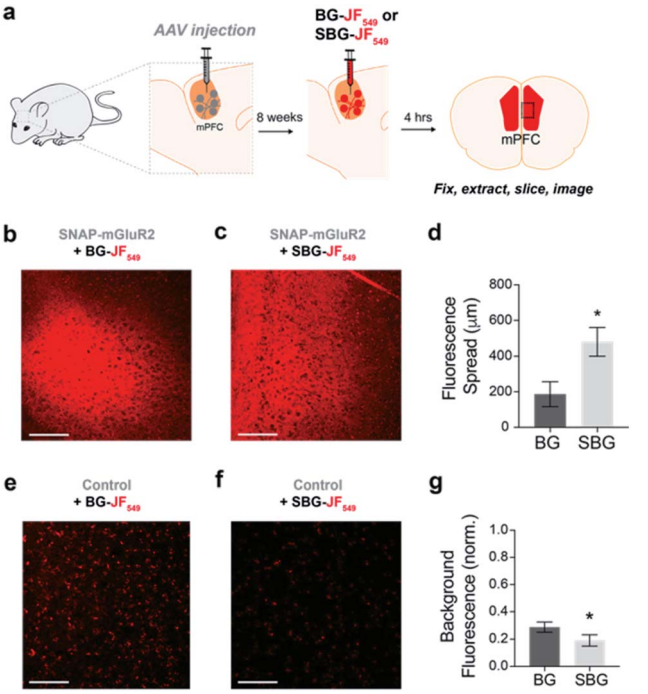

Fig. 3 *In vivo* labelling of a SNAP-tagged receptor with SBG-conjugated fluorophores produces less background and more spread. (a) Schematic showing AAV-mediated expression of SNAP-mGluR2 in the medial prefrontal cortex (mPFC) of mice, followed by SBG-JF_{549} or BG-JF_{549} dye injection and slice preparation 8 weeks later. (b and c) Representative images showing fluorescence in slices from SNAP-mGluR2 expressing mice following injection of BG (b) or SBG (c) fluorophores. (d) SBG-JF_{549} shows broader spread throughout the cortex compared to BG-JF_{549}. * indicates statistical significance (unpaired *t*-test, $p = 0.04$). (e and f) Representative images showing fluorescence in control slices following injection of BG (e) or SBG (f) fluorophores. (g) Larger background signals are observed for BG-conjugated dye. * indicates statistical significance (unpaired *t*-test, $p = 0.007$). Data is represented as mean ± SEM and comes from $n = 3$ mice for each condition. Labelling concentration was 1 μM. Scale bars are 150 μm.

noticed a cytosolic pool of SiR:SNAP-GLP1R, which either remained static and did not undergo trafficking, or alternatively, was degraded before being replenished by the portion of surface receptor labelled by SiR (Fig. 4d and e). Thus, GLP1R present at intracellular sites immediately before orthosteric activation are unlikely to make major contributions to ligand-induced receptor turnover. We next wondered if our technique could be used to probe the stoichiometry of GPCR populations inside the cell *versus* at the plasma membrane. Fluorescence-based methods have been widely used for assessing GPCR dimer- and oligomerization but rarely distinguish between surface and intracellular pools which may lead to confounding results and discrepancies across studies. This is especially critical as GPCR homo- and hetero-multimerization remains a controversial topic that may have major implications for general physiology and drug discovery.[33] We decided to use our labelling probes in conjunction with single molecule pulldown (SiMPull), a strategy which allows single receptor complexes to be isolated and imaged for analysis of stoichiometry *via* counting of fluorophore bleaching steps.[34] To probe a prototypical class C GPCR, reported to form constitutive dimers by most studies to date,[35,36] we used HA-SNAP-mGluR2. Conversely, an HA-SNAP-beta-2 adrenergic receptor construct ("HA-SNAP-β2AR") was used as a prototypical class A GPCR, which has been found as a monomer or dimer or higher order oligomer depending on experimental conditions.[34,37–41] Each construct was labeled with either SBG-JF_{549}, to label only surface receptors, or SNAP-Surface® Block followed by BG-JF_{549} (see methods for details) to isolate intracellular receptors. Cell imaging showed distinct fluorescence patterns for each receptor depending on the labelling paradigm (Fig. 5a) and labelling controls indicated that the BG-surface block prevented >95% of labelling of surface receptors without altering the efficiency of labelling intracellular receptors (Fig. S8a–d†). Following labelling, cells were lysed and detergent-solubilized GPCRs were isolated for single molecule imaging at a low density on passivated coverslips using an anti-HA antibody as previously described[42] (Fig. 5b). Single molecules were imaged using TIRF microscopy to allow for stepwise fluorophore bleaching which could be used to measure receptor stoichiometry (Fig. 5c). SBG-JF_{549} labeled HA-SNAP-mGluR2 showed ~55–60% 2-step photobleaching, consistent with previous studies indicating the formation of strict mGluR dimers.[35,36,42] However, intracellular receptors labeled with BG-JF_{549} showed reduced 2-step bleaching, indicating reduced dimerization in this population (Fig. 5d). These data suggest that a portion of the intracellular receptors are immature and monomeric.

We next performed the same experiment with HA-SNAP-β2AR (Fig. 5e and f). Consistent with our previous SiMPull study,[42] we found weak dimerization of surface receptors labelled with SBG-JF_{549} (Fig. 5g and h). However, when we targeted intracellular receptors a small, but significant increase in apparent dimerization was observed (Fig. 5h). Together these data demonstrate the suitability of SBG and BG dyes for isolating surface *versus* intracellular receptor pools for experiments that take place *in vitro* following cell lysis. In addition, they indicate that different receptor pools may have different distributions of monomeric and multimeric receptors, emphasizing the importance of identifying which pool is being probed in a given study.

Finally, we wondered if we could use dual labelling of surface and intracellular populations with two colours to assess the dimer stability of isolated receptors. First, as a control we labelled HA-SNAP-mGluR2 expressing cells with SBG-JF_{549} and SBG-JF_{646} and observed overlapping surface-labelling in both colours (Fig. 5i). In contrast, when we labelled surface receptors with SBG-JF_{549} followed by intracellular receptors with BG-JF_{646}, there was a clear discrepancy between the two colours in terms of cellular targeting (Fig. 5i). We next lysed cells and isolated receptors for single molecule imaging. In the first condition with both dyes conjugated to SBG, ~20% of spots were co-localized, consistent with substantial co-labelling of surface dimers (Fig. 5j, k and S8e†). In contrast, when one SBG- and one BG-conjugated fluorophore was used there was essentially no (~2%) co-localization (Fig. 5j, k and S8e†). This indicates that surface and intracellular receptor pools remain distinct

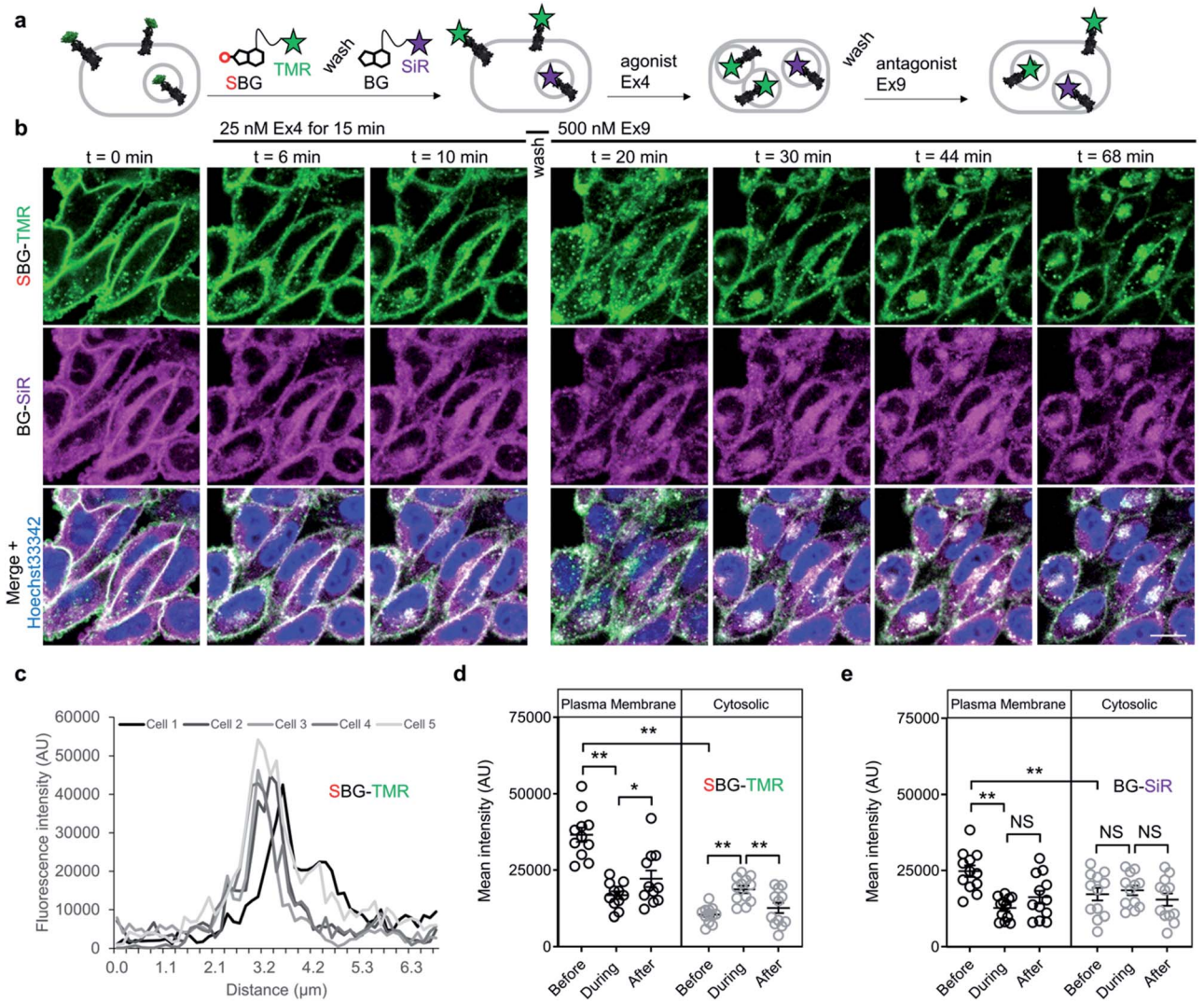

Fig. 4 SBG and BG-conjugated fluorophores allow tracking of different receptor pools in live cells. (a) Surface GLP1R is labelled with SBG-TMR, before washing and labelling of cytosolic receptor (and residual or newly trafficked receptor) with BG-SiR. The two GLP1R pools are then tracked over time in response to agonist stimulation (Ex4, exendin 4(1–39); 25–50 nM), followed by washing and antagonist application (Ex9, exendin 9(9–39); 500 nM) to halt trafficking. (b) Cytosolic GLP1R (BG-SiR) remains relatively static, while surface GLP1R (SBG-TMR) reversibly internalizes (representative images shown) (scale bar = 34 μm) (nuclei are labelled with Hoechst 33342). (c) SBG-TMR labelling at the membrane is homogenous between cells within the same preparation under non-stimulated conditions (n = 5 cells). (d and e) Quantification of mean fluorescence intensity at the plasma membrane and within the cytosol, showing significant changes in cytosolic SBG-TMR (d), but not BG-SiR (e), signal before (0 min), during (11–17 min) and after (53–61 min) agonist stimulation (repeated measures two-way ANOVA, Fishers LSD or Bonferonni's post-hoc test) (n = at least 2 different imaging positions in 6–9 wells, 3 independent repeats). *P < 0.05, **P < 0.01, NS, non-significant.

following lysis, and demonstrates the dual labelling and isolation of multiple receptor populations using bright fluorophores.

Discussion

The ability to specifically target surface proteins for imaging applications is critical for understanding receptor biology. To date, different approaches have been used to specifically label and interrogate membrane-spanning proteins at the extracellular side with a fluorescent tag. A traditional and powerful strategy is targeting native or tagged proteins with fluorophore-bearing antibodies (and their fragments),[43–45] nanobodies[27,46] or small molecules.[47–49] These approaches require new design and synthesis for each protein of interest, greatly limiting generalizability. In addition, how these probes affect the target protein's physiological roles (*i.e.* binding, trafficking and signalling) needs to be carefully examined on a case-to-case basis. The use of fluorescent protein-tagging of membrane proteins is more easily generalizable, but results in background staining as the protein construct folds and travels through the cell towards the surface or accumulates in internal compartments. To overcome this background, genetic approaches exist with proteins that are complemented on the cell surface and become fluorescent (*e.g.* split GFP[50]), or are endowed with an impermeable non-covalent fluorescent binder or ligand (for example, FRB-targeting probes[51] or the fluorescence-activating and

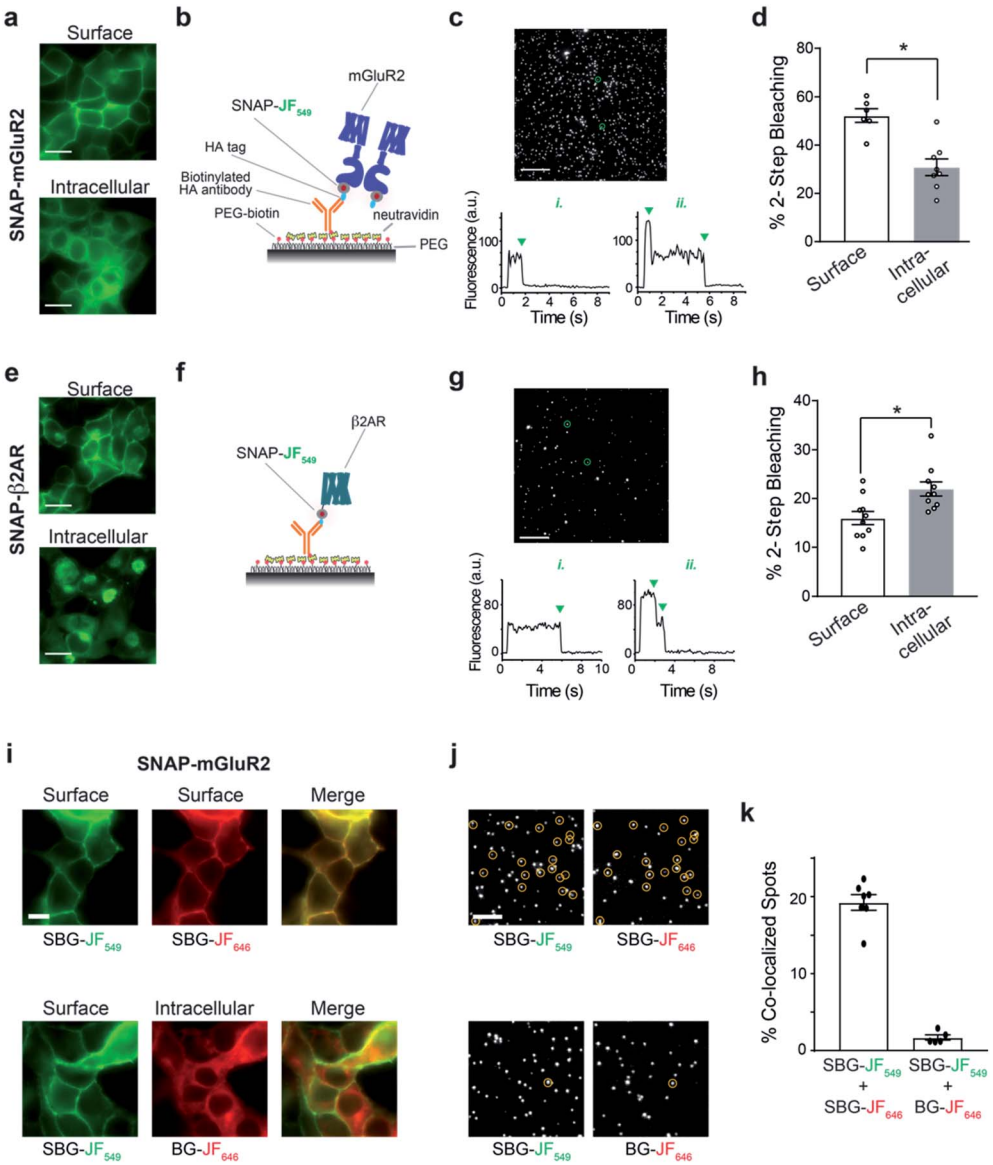

Fig. 5 BG and SBG-conjugated fluorophores enable SiMPull analysis of isolated surface or intracellular receptor populations. (a) Representative images showing labelling of either surface (top) or intracellular (bottom) SNAP-mGluR2 with SBG- or SNAP-Surface® Block followed by BG-JF_{549}, respectively. (b) Schematic showing single molecule pulldown configuration where an anti-HA antibody is used to isolate a sparse surface of SNAP-tagged mGluR2 following fluorophore labelling. (c) Representative image of single molecules for SNAP-mGluR2, with representative bleaching traces for a 1-step and 2-step example (bottom). Note: >95% of spots bleached in either 1 or 2-steps. (d) Summary of the proportion of 2-step bleaching steps for each labelling configuration. Each point represents one independent movie and bars show mean ± SEM. * indicates statistical significance (unpaired *t* test, $p = 0.0005$). (e–h) Same as (a–d) but with SNAP-β2AR. * indicates statistical significance (unpaired *t* test, $p = 0.008$). Scale bars are 10 μm. (i) Representative images showing 2-colour labelling of either surface SNAP-mGluR2 exclusively (top) or surface and intracellular SNAP-mGluR2 (bottom). All fluorophores were applied at 1 μM. (j) Representative images of single molecules in two different colours, with co-localized spots circled. (k) Summary of the proportion of total spots that are co-localized between the two colours. Each point represents one independent movie and bars show mean ± SEM.

absorbance-shifting tag (FAST)[52]). However, such fluorescent protein-based approaches are limited by poor photophysical properties, as most fluorescent proteins do not favourably compare to organic small molecule dyes,[53] and are therefore not amenable for certain experiments, such as single molecule microscopy or imaging at red or far-red wavelengths. The use of organic dyes can overcome these limitations due to their higher brightness and photostability, and are favourably used in superresolution microscopy or single molecule characterization. Installing an organic fluorophore on a protein target can be achieved in several ways, such as by cysteine–maleimide chemistry[54] or incorporation of unnatural amino acids and subsequent click chemistry,[55] which suffer from lack of specificity or efficiency and ease-of-use, respectively. For this reason, enzymatic labelling systems (*e.g.* ACP-tag,[56] "Sortagging"[57]) and self-labelling proteins (*i.e.* SNAP, CLIP, Halo) fused to the

protein target is the most widely used way to covalently attach a fluorescent substrate for surface labelling (the TMP-tag is an option for high-affinity, non-covalent labelling[58]). However, enzymatic systems are limited to membrane protein labelling, excluding labelling of intracellular pools. While many impermeable dyes exist and can be obtained commercially for self-labelling tags, they often lead to intracellular background staining and have non-ideal spectral or photophysical properties compared to permeable dyes (*e.g.* brightness: SulfoCy3 *vs.* JF_{549} compares 23 *vs.* 118). This raises the need for a general technique to control the membrane permeability of a dye at will.

We have rationally designed a modification to the BG leaving group to yield sulfonated-BG (SBG) that renders a range of *a priori* permeable fluorophores impermeable towards the plasma membrane. As such, the fluorophore remains identical after labelling, without alteration of its spectral or other photophysical properties. It should be noted that derivatizing the leaving group is possible for nucleobases as used for SNAP, but not for the leaving group of the Halo-tag, being a chloride atom. Recent approaches have used charged moieties synthetically introduced between the leaving group and the dye,[59] with the need to test for influences on binding kinetics and fluorogenicity, the latter which is optimized for the protein surface it is exposed to. Another approach is the use of inherently impermeable dyes, such as some Alexa, ATTO or Abberior, which display properties different to the dyes we aimed to use. Other impermeable modifications, such as relatively large quenchers custom-tailored for the fluorophore, have been reported for no-wash labelling of charged fluorophores.[60] In contrast, we describe a minimal alteration, independent of the cargo, that should be generally applicable.

Using our cell-impermeable SNAP substrates, we showcase fast and clean membrane staining of SNAP-mGluR2, accompanied by STED nanoscopy. By using SBG-linked bright and photostable dyes, we could restrict labelling to the lipid bilayer for different dyes in the visible spectrum. We furthermore obtained highly resolved images of SNAP-mGluR2 residing at the membrane using STED in fixed cells, which proved to be impossible after using the BG-version due to high intracellular background staining. The most stable and widely used far-red STED dyes (Atto 647N, STAR RED and STAR 635/P) are neither membrane permeable nor fluorogenic and hence cannot be used in cases where a comparison between intracellular and extracellular ligands is needed. On the other hand, the best performing dyes for live STED imaging (SiR, JF_{646}, CP 610) have been designed to ensure membrane permeability[9,24,61] and, therefore, they also do not allow for a comparison between intracellular and membrane protein pools, which necessarily requires the use of SBG-ligands.

JF_{549} showed superior behaviour when applied as its SBG-version *in vivo*. After application *via* injection, SBG-JF_{549} showed a 2-fold reduction in background when compared to its BG-congener. In contrast, its spread in virally-infected brains was markedly increased. These results, in addition to the ability to solubilize dyes without a co-solvent (*i.e.* DMSO), demonstrate the power of our simple chemical modification for use in living animals.

We were also able to stain a SNAP-GLP1R fusion construct at the membrane with SBG-TMR and the remaining, mostly intracellular, pool with BG-SiR. Separating pools of the same protein has been achieved before, for instance by using fluorogen-activated protein (FAP)[62,63] probes, the fluorescence-activating and absorbance-shifting tag (FAST)[52] and Halo-tag.[64] While these previous studies rely on non-covalent labelled protein tags fused to the BK channel or a transmembrane helix, respectively, we report a SNAP-fusion to a widely-drugged GPCR. In addition, our system does not rely on Förster Resonance Energy Transfer (FRET), which adds another layer of complexity and need for additional control experiments, as has been shown for malachite green conjugates. Furthermore, our approach allows for the use of different colours in the same experiment, while the FAST system uses charged and non-charged forms of the same fluorophores. As such, we show that GLP1R present at the membrane before ligand stimulation has increased propensity for trafficking in response to activation. By contrast, GLP1R which is already present inside the cell prior to stimulation does not appear to reach the membrane. As such, two pools of GLP1R likely exist in the unstimulated state: (1) surface-exposed receptor which is trafficking-competent in the presence of ligand; and (2) internalized, cytoplasmic, newly-synthesized or incorrectly processed GLP1R, which slowly traffics to the membrane in the absence of ligand or is, alternatively, degraded and replenished by labelled residual membrane receptor. Since peptide ligand cannot enter the cell, it is unlikely that the internalized GLP1R pool contributes meaningfully to intracellular (*e.g.* endosomal) signalling responses. What is the relevance of these observations for GLP1R function? Firstly, the initial surface GLP1R pool might turnover during ligand stimulation, with the initial intracellular pool never making it to the membrane within the timescale assessed here (*i.e.* measuring dynamic changes after activation). Secondly, ligands or allosteric modulators that can also target the intracellular GLP1R pool might further increase efficacy of GLP1R agonists used in the treatment of metabolic disease. Such complexity in receptor trafficking has not been detailed in living cells, validating our SBG-conjugated fluorophore approach.

Finally, we also demonstrate the value of the SBG approach for chemically-tagging surface receptors for subsequent biochemical isolation. We use this to show that SBG-targeted surface GPCRs can display different stoichiometries than BG-targeted intracellular GPCRs. In the case of the class C GPCR mGluR2, intracellular receptors, presumably immature proteins, show reduced dimerization compared to the strict dimerization of the cell surface population. In contrast, intracellular β2AR showed enhanced dimerization compared to surface pools. Critically, the ability to use the same fluorophore (JF_{549}) for each condition removes any possibility that differences in photobleaching pattern are due to differences in dye photophysics. Future work will be needed to dissect the determinants of the differential dimerization of these populations, their sensitivity to different stimuli and to assess this phenomenon across a range of GPCRs and other membrane proteins. The flexible control afforded by SBG-conjugated fluorophores will be critical for such studies.

We envision such an approach will be useful not only for fluorophore attachment, but also for purification of distinct receptor pools from the same sample or for adding tethered ligands to manipulate distinct populations.[29]

Conclusions

In conclusion, we report the design and use of novel highly-soluble and membrane impermeable probes for the interrogation of different GPCRs from the purified protein level to live cells to the whole organism.

Methods

Synthesis

Chemical synthesis (ESI Schemes S1 and S2†) and characterization of compounds is outlined in the ESI.† Purity of all CBG/SBG-linked dyes was determined to be of >95% by UPLC-UV/Vis traces at 254 nm and dye specific λ_{max} that were recorded on a Waters H-class instrument equipped with a quaternary solvent manager, a Waters autosampler, a Waters TUV detector and a Waters Acquity QDa detector with an Acquity UPLC BEH C18 1.7 μm, 2.1 × 50 mm RP column (Waters Corp., USA).

Excitation and emission profiles of CBG/SBG-linked dyes

Excitation and emission profiles were recorded on a TECAN infinite 2000Pro plate reader. Stocks of SNAP substrates (20 μM in DMSO) were diluted to 200 nM into PBS containing 10 μg mL^{-1} BSA in a Greiner black flat bottom 96 well plate before reading was started with 15 flashes and 20 μs integration time. Wavelengths and ranges are summarized in Table S1.† Experiments were run in quadruplicate, data was normalized and the mean was plotted in GraphPad Prism 8.

Statistical analysis

GraphPad Prism or Excel software was used for all data analysis. Pairwise comparisons were performed using two-sided students *t*-test. Multiple interactions were determined using two-way ANOVA followed by Bonferonni's or Fisher's LSD post-hoc tests.

$SNAP_f$ expression, purification, and mass spectrometry after labelling

$SNAP_f$ was expressed and purified as described previously.[27] Briefly, $SNAP_f$ with an N-terminal Strep-tag and C-terminal 10× His-tag was cloned into a pET51b(+) expression vector for bacterial expression and complete amino acid sequences for constructs used can be found in the ESI.† For purification, $SNAP_f$ was expressed in the *E. coli* strain BL21 pLysS. LB media contained ampicillin (100 μg mL^{-1}) for protein expression. A culture was grown at 37 °C until an OD_{600} of 0.6 was reached at which point cells were induced with IPTG (0.5 mM). Protein constructs were expressed overnight at 16 °C. Cells were harvested by centrifugation and sonicated to produce cell lysates. The lysate was cleared by centrifugation and purified by Ni-NTA resin (Thermo Fisher) and Strep-Tactin II resin (IBA) according to the manufacturer's protocols. Purified protein samples were stored in 50 mM HEPES, 50 mM NaCl (pH 7.3) and either flash frozen and stored at −80 °C. For $SNAP_f$ labelling, 25 μL of 30 μM dye (BG/SBG-TMR) in activity buffer (50 mM HEPES, 50 mM NaCl, pH = 7.3) was added to a 10 μM solution of $SNAP_f$ in activity buffer in 1.5 mL Eppendorf tubes. This resulted in a 3-fold excess of labelling substrate and mixing was ensured by carefully pipetting the solution up and down. The reaction mixture was allowed to incubate at r.t. for 1 h before tubes were stored at 4 °C until MS analysis.

$SNAP_f$ labelling kinetics

Kinetic measurements were performed on a TECAN Spark 20M platereader by means of fluorescence polarization. Stocks of $SNAP_f$ (400 nM) and TMR substrates (100 nM) were prepared in activity buffer: 50 mM HEPES, 50 mM NaCl, 1 mM DTT, 100 ng mL^{-1} BSA, pH = 7.3. $SNAP_f$ and substrates were mixed (50 μL each) in a Greiner black flat bottom 96 well plate and fluorescence polarization reading was started immediately (λ_{Ex} = 535 ± 25 nm; λ_{Em} = 595 ± 35 nm; 30 flashes; 40 μs integration time). Experiments were run in triplicates, data was normalized and one-phase decay fitted in GraphPad Prism 7.

Solubility studies

Lyophilized compounds were dissolved in PBS (SBG-TMR) or in DMSO (BG-TMR). Concentration was assessed by diluting each 1 : 50 into PBS/0.1% SDS and measuring UV absorbance at 550 nm by a NanoDrop (extinction coefficient: 90 000 M^{-1} cm^{-1}; pathlength d = 0.1 cm) to be in the single digit millimolar range. BG-TMR was diluted 1 : 100 in PBS and aliquoted into 1.5 mL Eppendorf tubes, which were spun at 15 000 rpm for 30 seconds, the supernatant diluted 1 : 1 with PBS/0.1% SDS and concentration determined at a NanoDrop. Time intervals were 0, 7, 14, 21 and 40 min. SBG-TMR was diluted 1 : 25 in PBS and aliquoted into 1.5 mL Eppendorf tubes, which were spun at 14 600 rpm for 30 seconds, the supernatant diluted 1 : 1 with PBS/0.1% SDS and concentration determined at a NanoDrop. Time intervals were 0, 7, 14, 21, 40 min and after 3 days (4320 min).

Cell lines

CHO-K1 cells stably expressing SNAP-GLP1R (CHO-K1_SNAP-GLP1R) were generated by and obtained from Dr Ben Jones, Imperial College London, UK. HEK 293 and HEK 293T cells were purchased from ATCC: 293 [HEK-293] (ATCC® CRL-1573™) and 293T/17 [HEK 293T/17] (ATCC® CRL-11268™). All cell lines were regularly tested for mycoplasma.

Expression and fluorescence imaging in HEK 293T cells

HEK 293T cells were cultured in DMEM with 5% FBS, seeded on 18 mm poly-L-lysine-coated cover slips in a 12-well plate and transfected using lipofectamine 2000 (Thermo Scientific). Cells were transfected with 0.3–0.7 μg per well of SNAP-tagged constructs.

After 24–48 h of expression, cells were first washed with extracellular (EX) solution containing (in mM): 10 HEPES, 135

NaCl, 5.4 KCl, 2 $CaCl_2$, 1 $MgCl_2$, pH 7.4 and labeled with fluorophores at 37 °C at the indicated concentrations for 45 min. Cells were washed at least three times before imaging. An inverted microscope (Olympus IX83) was used for fluorescence imaging. Live cell images were captured using a 60× objective (NA 1.49) with an exposure time of 100 ms. Laser intensity was kept constant across the compared samples for fluorescence intensity quantification. Average fluorescence intensity from cell images was measured using ImageJ by drawing a region of interest (ROI) around cell clusters. Fluorescence intensity values from multiple images were then averaged. Each condition was tested in at least 2 separate transfections. All images that were directly compared were obtained under identical conditions, *i.e.* on the same day from the same batch of cells and imaged using identical laser power, optical settings and exposure times. For each condition 5–10 images were collected and fluorescence was analyzed in ImageJ by drawing a region of interest around cell clusters (5–20 cells; 2–3 per field of view) to measure the average pixel. Background levels from regions without cells were subtracted for each image and the intensity values were averaged for each condition across all ROIs and normalized to a standard condition. 2 separate days are averaged for all experiments in Fig. 1 and all data in Fig. 2 comes from one day of experiments per condition. Fluorescence (norm.) stands for total fluorescence of the cluster.

Superresolution microscopy

HEK 293 cells transfected with SNAP-mGluR2 growing on 18 mm coverslips were treated with 400 nM BG-JF_{646} or SBG-JF_{646} for 60 min in DMEM (without phenol red), washed and fixed (4% paraformaldehyde for 20 min, followed by quenching solution 0.1 M glycine, 0.1 M NH_4Cl in PBS). Cells were mounted in mowiol supplemented with DABCO and imaged on an Abberior STED 775/595/RESOLFT QUAD scanning microscope (Abberior Instruments GmbH, Germany) equipped with STED lines at $\lambda = 595$ and $\lambda = 775$ nm, excitation lines at $\lambda =$ 355 nm, 405 nm, 485 nm, 561 nm, and 640 nm, spectral detection, and a UPlanSApo 100×/1.4 oil immersion objective lens. Following excitation at $\lambda = 640$ nm, fluorescence was acquired in the spectral window $\lambda = 650$–800 nm. FWHM was measured on raw data and calculated using Fiji software with Gaussian fitting.

Fluorescence lifetime microscopy

CHO-K1 cells stably expressing the human SNAP-GLP1R (Cisbio) (CHO-K1_SNAP-GLP1R) were maintained in DMEM supplemented with 10% FCS, 1% penicillin/streptomycin, 500 μg mL^{-1} G418, 25 mM HEPES, 1% nonessential amino acids and 2% L-glutamine. Cells were incubated with 1 μM BG-JF_{549} or SBG-JF_{549} for 30 min at 37 °C, 5% CO_2, before washing three times in medium. Live cell fluorescence lifetime microscopy was performed using a Leica SP8 with FALCON (Leica Microsystems) equipped with a pulsed white-light excitation laser (80 MHz repetition rate (NKT Photonics)), a 100× objective (HC PL APO CS2 100×/1.40 NA oil), a temperature controlled chamber and operated by LAS X. SNAP-JF_{549} was excited using $\lambda = 561$ nm. Emission signals were captured at $\lambda = 576$–670 nm using a Hybrid detector producing FLIM images of 512 × 512 pxl with 113 nm per pxl and 16 repetitions. Fluorescence lifetime decay curves from selected regions with clear plasma membrane staining were fitted with two exponential functions and the mean amplitude weighted lifetime is reported for each region.

Mice

All animal use procedures were performed in accordance with the Guidelines for "Care and Use of Laboratory Animals" of Weill Cornell Medicine Institution with guidelines under approved protocol by the "Animal Care & Use Committee (IACUC)" of Weill Cornell Medicine (2017-0023). Male wild-type mice were of strain C57BL/6J and purchased from Jackson Laboratory and were maintained under specific pathogen free conditions at the Weill Cornell Medicine Animal Facility. Animals were provided food and water *ad libitum* and housed in a temperature and humidity-controlled environment with a 12 hour light/12 hour dark cycle.

In vivo SNAP labelling

AAV-mediated expression of SNAP-mGluR2 and *in vivo* SNAP labelling was performed as previously described.[29] Briefly, male C57BL/6J mice were injected at p60 with a 1:1 viral cocktail of AAV9-EF1a-FLEX-SNAP-mGluR2-WPRE-hGH (Penn Vector Core) and pENN-AAV9-CamKII 0.4-Cre-SV40 (Addgene) or, as a control, only AAV9-EF1a-FLEX-SNAP-mGluR2-WPRE-hGH. Mice were injected in the medial prefrontal cortex (AP +1.85, ML ±0.35, DV −2.2, −1.8) with 500 nL per site using a Kopf stereotaxic and World Precision Instruments microinjection syringe pump with a 10 μL syringe and 33G blunt needle. 8 weeks after viral injection, mice received infusion of 500 nL of 1 μM BG-JF_{549} or SBG-JF_{549} targeted to the same site as viral injection. 4 hours later mice underwent transcardial perfusion and were fresh fixed with 4% paraformaldehyde. Brains were extracted and bathed in 4% paraformaldehyde for 24 hours followed by 72 hours in 30% sucrose PBS solution. Brains were mounted and frozen at −20 °C in OCT block and medial prefrontal cortex was sliced at 40 μm thick on a cryostat at −22 °C. Slices were wet mounted to glass slides and secured with coverslip using VECTASHIELD HardSet Antifade Mounting Medium with DAPI (Vector Laboratories). Glass slides were imaged using an Olympus Confocal FV3000 and images were processed and analyzed in ImageJ.

GLP1R trafficking studies

CHO-K1 cells stably expressing the human SNAP-GLP1R (Cisbio) (CHO-K1_SNAP-GLP1R) were maintained in DMEM supplemented with 10% FCS, 1% penicillin/streptomycin, 500 μg mL^{-1} G418, 25 mM HEPES, 1% nonessential amino acids and 2% L-glutamine. Cells were incubated with 500 nM SBG-TMR for 15 min at 37 °C, 5% CO_2, before washing three times in medium. BG-SiR was then applied at 500 nM for 20 min under the same conditions. Live imaging was performed using a Zeiss LSM880 meta-confocal microscope configured with GaAsP detectors, a 63×/1.2 W Korr M27 objective and a temperature and CO_2-controlled chamber. Exendin 4(1–39) (25 nM) and exendin 4(9–

39) (500 nM) were applied at the indicated timepoints and concentrations. SNAP-TMR, SNAP-SiR and Hoechst 33342 were excited using $\lambda = 561$ nm, $\lambda = 633$ nm and $\lambda = 405$ nm lasers, respectively. Emitted signals were captured at $\lambda = 569$–614 nm, $\lambda = 641$–694 nm and $\lambda = 410$–520 nm for SNAP-TMR, SNAP-SiR and Hoechst 33342, respectively. Control experiments were performed in either SBG-TMR- or BG-SiR-labelled cells to exclude trafficking artefacts due to spectral overlap.

Single molecule pulldown assay

Single molecule pulldown (SiMPull) was performed using HA-tagged GPCRs isolated on glass coverslips as previously described using a biotinylated anti-HA antibody.[42] Briefly, flow chambers were prepared with mPEG-passivated glass slides and coverslips with ~1% biotinylated PEG to allow antibody capture. Prior to each experiment, flow chambers were incubated with 0.2 mg mL^{-1} NeutrAvidin for 2 min then incubated with 10 nM of antibody (abcam, ab26228) for 30 min. The flow chambers were rinsed with T50 buffer (50 mM NaCl, 10 mM Tris, pH 7.5) after each conjugation step. Cell lysate was prepared 24–48 hours after transfection with HEK 293T cells and immediately after labelling at 37 °C with either with 1 μM SBG-JF_{549} for 45 minutes or 20 μM SNAP-Surface® Block (NEB) followed by 1 μM BG-JF_{549} for 45 min each. For 2-colour experiments, either SBG-JF_{549} and SBG-JF_{646} were simultaneously applied or SBG-JF_{549} was applied followed by BG-JF_{646}. After extensive washing with EX solution (in mM, 10 HEPES, 135 NaCl, 5.4 KCl, 2 $CaCl_2$, 1 $MgCl_2$, pH 7.4), cells were harvested using Ca^{2+} free-DPBS for 20 min at 37 °C. After pelleting the cells at 10 000×*g*, 4 °C for 1 min, cells were lysed using 1.2% IGEPAL detergent for 1 hour at 4 °C. Next, cells were centrifuged at 16 000×*g* for 20 min at 4 °C and supernatant was collected and stored in ice until used. The cell lysate samples were then diluted using a dilution buffer containing 0.1% IGEPAL and introduced to the flow chamber. After obtaining an optimal number of spots in the field of view, the chamber was washed with the dilution buffer to remove unbound proteins.

Single molecule imaging was done using a 100× objective (NA 1.49) on an inverted microscope (Olympus IX83) in total internal reflection (TIR) mode at 20 Hz with 50 ms exposure times with an sCMOS camera (Hamamatsu ORCA-Flash4v3.0). Samples were excited with 561 nm or 640 nm lasers and imaged using emission filters of 595 ± 25 nm or 655 nm long pass, respectively. Data analysis was performed using custom made LabVIEW program as previously described.[65] Data was collected across at least 2 separate experimental days and then averaged to produce bar graphs in Fig. 5d and h.

Conflicts of interest

There are no conflicts to declare.

Acknowledgements

We thank Andrea Bergner for providing purified $SNAP_f$ protein, Kai Johnsson and Birgit Koch for SNAP plasmids, Sebastian Fabritz and Cornelia Ullrich for small molecule and full protein mass spectrometry, Kai Johnsson for support and Philipp Leippe for helpful discussion (all MPIMR). We are further grateful to Jenny Eichhorst for FLIM, and to Corentin Charbonnier for *in vitro* measurements, Peter Schmieder for ^1H NMR and the Hackenberger Lab for support (all FMP). D. J. H. was supported by a Diabetes UK R. D. Lawrence (12/0004431) Fellowship, and MRC (MR/N00275X/1 and MR/S025618/1) and Diabetes UK (17/0005681) Project Grants. This project has received funding from the European Research Council (ERC) under the European Union's Horizon 2020 Research and Innovation Programme (Starting Grant 715884 to D. J. H.). JL is supported by an R35 grant (1 R35 GM124731) from NIGMS and the Rohr Family Research Scholar Award.

Notes and references

1 B. Alberts, A. Johnson, J. Lewis, M. Raff, K. Roberts and P. Walter, *Molecular Biology of the Cell*, Garland Science, vol. 5, 2007.
2 A. S. Hauser, M. M. Attwood, M. Rask-Andersen, H. B. Schiöth and D. E. Gloriam, *Nat. Rev. Drug Discovery*, 2017, **16**, 829–842.
3 M. A. Lemmon and J. Schlessinger, *Cell*, 2010, **141**, 1117–1134.
4 K. Eichel and M. von Zastrow, *Trends Pharmacol. Sci.*, 2018, **39**, 200–208.
5 H. Xu, E. Martinoia and I. Szabo, *Cell Calcium*, 2015, **58**, 1–10.
6 B. O'Rourke, *Annu. Rev. Physiol.*, 2007, **69**, 19–49.
7 L. D. Lavis, *Annu. Rev. Biochem.*, 2017, **86**, 825–843.
8 L. Wang, M. Tran, E. D'Este, J. Roberti, B. Koch, L. Xue and K. Johnsson, *Nat. Chem.*, 2020, **12**, 165–172.
9 A. N. Butkevich, G. Y. Mitronova, S. C. Sidenstein, J. L. Klocke, D. Kamin, D. N. H. Meineke, E. D'Este, P.-T. Kraemer, J. G. Danzl, V. N. Belov and S. W. Hell, *Angew. Chem., Int. Ed.*, 2016, **55**, 3290–3294.
10 L. Wang, M. S. Frei, A. Salim and K. Johnsson, *J. Am. Chem. Soc.*, 2019, **141**, 2770–2781.
11 L. Xue, I. A. Karpenko, J. Hiblot and K. Johnsson, *Nat. Chem. Biol.*, 2015, **11**, 917–923.
12 S. Benson, A. Fernandez, N. D. Barth, F. de Moliner, M. H. Horrocks, C. S. Herrington, J. L. Abad, A. Delgado, L. Kelly, Z. Chang, Y. Feng, M. Nishiura, Y. Hori, K. Kikuchi and M. Vendrell, *Angew. Chem., Int. Ed.*, 2019, **58**, 6911–6915.
13 C. Deo, S.-H. Sheu, J. Seo, D. E. Clapham and L. D. Lavis, *J. Am. Chem. Soc.*, 2019, **141**, 13734–13738.
14 P. Scholler, D. Moreno-Delgado, N. Lecat-Guillet, E. Doumazane, C. Monnier, F. Charrier-Savournin, L. Fabre, C. Chouvet, S. Soldevila, L. Lamarque, G. Donsimoni, T. Roux, J. M. Zwier, E. Trinquet, P. Rondard and J.-P. Pin, *Nat. Chem. Biol.*, 2017, **13**, 372–380.
15 R. Vafabakhsh, J. Levitz and E. Y. Isacoff, *Nature*, 2015, **524**, 497–501.
16 D. Maurel, L. Comps-Agrar, C. Brock, M.-L. Rives, E. Bourrier, M. A. Ayoub, H. Bazin, N. Tinel, T. Durroux,

L. Prézeau, E. Trinquet and J.-P. Pin, *Nat. Methods*, 2008, **5**, 561–567.
17 T. Klein, A. Löschberger, S. Proppert, S. Wolter, S. van de Linde and M. Sauer, *Nat. Methods*, 2011, **8**, 7–9.
18 A. R. B. Thomsen, B. Plouffe, T. J. Cahill, A. K. Shukla, J. T. Tarrasch, A. M. Dosey, A. W. Kahsai, R. T. Strachan, B. Pani, J. P. Mahoney, L. Huang, B. Breton, F. M. Heydenreich, R. K. Sunahara, G. Skiniotis, M. Bouvier and R. J. Lefkowitz, *Cell*, 2016, **166**, 907–919.
19 T. Sungkaworn, M.-L. Jobin, K. Burnecki, A. Weron, M. J. Lohse and D. Calebiro, *Nature*, 2017, **550**, 543–547.
20 S. A. Jones, S.-H. Shim, J. He and X. Zhuang, *Nat. Methods*, 2011, **8**, 499–508.
21 B. Barlag, O. Beutel, D. Janning, F. Czarniak, C. P. Richter, C. Kommnick, V. Göser, R. Kurre, F. Fabiani, M. Erhardt, J. Piehler and M. Hensel, *Sci. Rep.*, 2016, **6**, 1–14.
22 C. P. Toseland, *J. Chem. Biol.*, 2013, **6**, 85–95.
23 L. D. Hughes, R. J. Rawle and S. G. Boxer, *PLoS One*, 2014, **9**, e87649.
24 J. B. Grimm, B. P. English, J. Chen, J. P. Slaughter, Z. Zhang, A. Revyakin, R. Patel, J. J. Macklin, D. Normanno, R. H. Singer, T. Lionnet and L. D. Lavis, *Nat. Methods*, 2015, **12**, 244–250.
25 C. T. H. Jonker, C. Deo, P. J. Zager, A. N. Tkachuk, A. M. Weinstein, E. Rodriguez-Boulan, L. D. Lavis and R. Schreiner, *J. Cell Sci.*, 2020, **133**, jcs231225.
26 T. Komatsu, K. Johnsson, H. Okuno, H. Bito, T. Inoue, T. Nagano and Y. Urano, *J. Am. Chem. Soc.*, 2011, **133**, 6745–6751.
27 H. Farrants, V. A. Gutzeit, A. Acosta-Ruiz, D. Trauner, K. Johnsson, J. Levitz and J. Broichhagen, *ACS Chem. Biol.*, 2018, **13**, 2682–2688.
28 J. B. Grimm, A. K. Muthusamy, Y. Liang, T. A. Brown, W. C. Lemon, R. Patel, R. Lu, J. J. Macklin, P. J. Keller, N. Ji and L. D. Lavis, *Nat. Methods*, 2017, **14**, 987–994.
29 A. Acosta-Ruiz, V. A. Gutzeit, M. J. Skelly, S. Meadows, J. Lee, P. Parekh, A. G. Orr, C. Liston, K. E. Pleil, J. Broichhagen and J. Levitz, *Neuron*, 2020, **105**, 446–463.e13.
30 T. Podewin, J. Ast, J. Broichhagen, N. H. F. Fine, D. Nasteska, P. Leippe, M. Gailer, T. Buenaventura, N. Kanda, B. J. Jones, C. M'Kadmi, J.-L. Baneres, J. Marie, A. Tomas, D. Trauner, A. Hoffmann-Röder and D. J. Hodson, *ACS Cent. Sci.*, 2018, **4**, 166–179.
31 S. N. Roed, P. Wismann, C. R. Underwood, N. Kulahin, H. Iversen, K. A. Cappelen, L. Schäffer, J. Lehtonen, J. Hecksher-Soerensen, A. Secher, J. M. Mathiesen, H. Bräuner-Osborne, J. L. Whistler, S. M. Knudsen and M. Waldhoer, *Mol. Cell. Endocrinol.*, 2014, **382**, 938–949.
32 B. Jones, T. Buenaventura, N. Kanda, P. Chabosseau, B. M. Owen, R. Scott, R. Goldin, N. Angkathunyakul, I. R. Corrêa Jr, D. Bosco, P. R. Johnson, L. Piemonti, P. Marchetti, A. M. J. Shapiro, B. J. Cochran, A. C. Hanyaloglu, A. Inoue, T. Tan, G. A. Rutter, A. Tomas and S. R. Bloom, *Nat. Commun.*, 2018, **9**, 1602.
33 R. Sleno and T. E. Hébert, *Int. Rev. Cell Mol. Biol.*, 2018, **338**, 141–171.
34 A. Jain, R. Liu, B. Ramani, E. Arauz, Y. Ishitsuka, K. Ragunathan, J. Park, J. Chen, Y. K. Xiang and T. Ha, *Nature*, 2011, **473**, 484–488.
35 E. Doumazane, P. Scholler, J. M. Zwier, E. Trinquet, P. Rondard and J. P. Pin, *FASEB J.*, 2011, **25**, 66–77.
36 J. Levitz, C. Habrian, S. Bharill, Z. Fu, R. Vafabakhsh and E. Y. Isacoff, *Neuron*, 2016, **92**, 143–159.
37 S. Angers, A. Salahpour, E. Joly, S. Hilairet, D. Chelsky, M. Dennis and M. Bouvier, *Proc. Natl. Acad. Sci. U. S. A.*, 2000, **97**, 3684–3689.
38 T. E. Hebert, S. Moffett, J. P. Morello, T. P. Loisel, D. G. Bichet, C. Barret and M. Bouvier, *J. Biol. Chem.*, 1996, **271**, 16384–16392.
39 J. J. Fung, X. Deupi, L. Pardo, X. J. Yao, G. A. Velez-Ruiz, B. T. DeVree, R. K. Sunahara and B. K. Kobilka, *EMBO J.*, 2009, **28**, 3315–3328.
40 S. Mathiasen, S. M. Christensen, J. J. Fung, S. G. F. Rasmussen, J. F. Fay, S. K. Jorgensen, S. Veshaguri, D. L. Farrens, M. Kiskowski, B. Kobilka and D. Stamou, *Nat. Methods*, 2014, **11**, 931–934.
41 M. R. Whorton, M. P. Bokoch, S. G. F. Rasmussen, B. Huang, R. N. Zare, B. Kobilka and R. K. Sunahara, *Proc. Natl. Acad. Sci. U. S. A.*, 2007, **104**, 7682–7687.
42 V. A. Gutzeit, J. Thibado, D. S. Stor, Z. Zhou, S. C. Blanchard, O. S. Andersen and J. Levitz, *eLife*, 2019, **8**, e45116.
43 C. E. Fritze and T. R. Anderson, in *Methods in Enzymology*, ed. J. Thorner, S. D. Emr and J. N. Abelson, Academic Press, 2000, vol. 327, pp. 3–16.
44 H. Zhuang and H. Matsunami, *Nat. Protoc.*, 2008, **3**, 1402–1413.
45 M. Brown, L. J. Stafford, D. Onisk, T. Joaquim, A. Tobb, L. Goldman, D. Fancy, J. Stave and R. Chambers, *PLoS One*, 2013, **8**, e73255.
46 H. Götzke, M. Kilisch, M. Martínez-Carranza, S. Sograte-Idrissi, A. Rajavel, T. Schlichthaerle, N. Engels, R. Jungmann, P. Stenmark, F. Opazo and S. Frey, *Nat. Commun.*, 2019, **10**, 4403.
47 T. Hayashi and I. Hamachi, *Acc. Chem. Res.*, 2012, **45**, 1460–1469.
48 S. Karch, J. Broichhagen, J. Schneider, D. Böning, S. Hartmann, B. Schmid, P. Tripal, R. Palmisano, C. Alzheimer, K. Johnsson and T. Huth, *J. Med. Chem.*, 2018, **61**, 6121–6139.
49 J. Ast, A. Arvaniti, N. H. F. Fine, D. Nasteska, F. B. Ashford, Z. Stamataki, Z. Koszegi, A. Bacon, B. J. Jones, M. A. Lucey, S. Sasaki, D. I. Brierley, B. Hastoy, A. Tomas, G. D'Agostino, F. Reimann, F. C. Lynn, C. A. Reissaus, A. K. Linnemann, E. D'Este, D. Calebiro, S. Trapp, K. Johnsson, T. Podewin, J. Broichhagen and D. J. Hodson, *Nat. Commun.*, 2020, **11**, 467.
50 W.-X. Jiang, X. Dong, J. Jiang, Y.-H. Yang, J. Yang, Y.-B. Lu, S.-H. Fang, E.-Q. Wei, C. Tang and W.-P. Zhang, *Sci. Rep.*, 2016, **6**, 20568.
51 X. Zhang, Y. Deng, H. Chang, C. Ji, M. Zhang, J. Peng, T. Xu and P. Xu, *Protein Cell*, 2014, **5**, 800–803.
52 C. Li, A. Mourton, M.-A. Plamont, V. Rodrigues, I. Aujard, M. Volovitch, T. Le Saux, F. Perez, S. Vriz, L. Jullien,

A. Joliot and A. Gautier, *Bioconjugate Chem.*, 2018, **29**, 1823–1828.
53 E. C. Jensen, *Anat. Rec.*, 2012, **295**, 2031–2036.
54 J. Skalska, P. S. Brookes, S. M. Nadtochiy, S. P. Hilchey, C. T. Jordan, M. L. Guzman, S. B. Maggirwar, M. M. Briehl and S. H. Bernstein, *PLoS One*, 2009, **4**, e8115.
55 K. Lang and J. W. Chin, *Chem. Rev.*, 2014, **114**, 4764–4806.
56 N. George, H. Pick, H. Vogel, N. Johnsson and K. Johnsson, *J. Am. Chem. Soc.*, 2004, **126**, 8896–8897.
57 M. W. Popp, J. M. Antos, G. M. Grotenbreg, E. Spooner and H. L. Ploegh, *Nat. Chem. Biol.*, 2007, **3**, 707–708.
58 L. W. Miller, Y. Cai, M. P. Sheetz and V. W. Cornish, *Nat. Methods*, 2005, **2**, 255–257.
59 E. Prifti, L. Reymond, M. Umebayashi, R. Hovius, H. Riezman and K. Johnsson, *ACS Chem. Biol.*, 2014, **9**, 606–612.
60 X. Sun, A. Zhang, B. Baker, L. Sun, A. Howard, J. Buswell, D. Maurel, A. Masharina, K. Johnsson, C. J. Noren, M.-Q. Xu and I. R. Corrêa, *ChemBioChem*, 2011, **12**, 2217–2226.
61 G. Lukinavičius, K. Umezawa, N. Olivier, A. Honigmann, G. Yang, T. Plass, V. Mueller, L. Reymond, I. R. Corrêa Jr, Z.-G. Luo, C. Schultz, E. A. Lemke, P. Heppenstall, C. Eggeling, S. Manley and K. Johnsson, *Nat. Chem.*, 2013, **5**, 132–139.
62 C. P. Pratt, J. He, Y. Wang, A. L. Barth and M. P. Bruchez, *Bioconjugate Chem.*, 2015, **26**, 1963–1971.
63 M. Naganbabu, L. A. Perkins, Y. Wang, J. Kurish, B. F. Schmidt and M. P. Bruchez, *Bioconjugate Chem.*, 2016, **27**, 1525–1531.
64 J. C. Stüber, F. Kast and A. Plückthun, *ACS Chem. Biol.*, 2019, **14**, 1154–1163.
65 M. H. Ulbrich and E. Y. Isacoff, *Nat. Methods*, 2007, **4**, 319–321.